

Contents lists available at ScienceDirect

# **Cement and Concrete Composites**

journal homepage: www.elsevier.com/locate/cemconcomp



# Multiple-scale investigations on self-healing induced mechanical property recovery of ECC



Zhigang Zhang<sup>a,\*</sup>, Qian Zhang<sup>b,\*\*</sup>, Victor C. Li<sup>c</sup>

- <sup>a</sup> Key Laboratory of New Technology for Construction of Cities in Mountain Area (Chongqing University), Ministry of Education, Chongqing, 400045, PR China
- b Department of Civil and Environmental Engineering, FAMU-FSU College of Engineering, Florida State University, Tallahassee, FL 32310, USA
- <sup>c</sup> Department of Civil and Environmental Engineering, University of Michigan, Ann Arbor, MI, United States

#### ARTICLE INFO

Keywords: ECC Self-healing Mechanical property recovery Multi-scale Interfacial properties

#### ABSTRACT

The self-healing behavior of Engineered Cementitious Composites (ECC) has attracted much research in the past decade. Nonetheless, very few study attempted to reveal the underlying mechanism of self-healing induced mechanical recovery of pre-damaged ECC. In this paper, the influence of self-healing on the material properties of ECC was investigated on multiple length scales. Plausible underlying mechanisms of mechanical properties recovery of ECC are proposed. The results show obvious regaining of tensile/flexural properties of pre-damaged ECC at macro-scale due to self-healing. At the meso-scale, self-healing leads to fiber bridging strength recovery to about the same level as that of virgin specimens. At the micro-scale, self-healing is found associated with recovery of frictional bond strength between the fiber and matrix. However, chemical bond recovery appears to be absent. The regaining in fiber/matrix interfacial friction results in the recovery of fiber bridging capacity, which forms the root cause for recovery of the mechanical properties of self-healed ECC.

#### 1. Introduction

Concrete is the most widely used construction materials in the field of civil engineering because of the wide availability and inexpensive raw ingredients worldwide. However, the inherent brittleness of concrete makes it prone to cracking when subjected to mechanical loading and/or environmental loading such as restrained drying shrinkage, freezing-and-thawing cycles, and sulfate attack. The appearance of cracks in concrete results in the loss of mechanical performance and poor durability, as cracks create channels for water and aggressive ions, such as chloride ion, to penetrate the concrete cover and enter the concrete structure interior [1,2]. The presence of aggressive ions causes corrosion and expansion of the steel rebar that generates tensile stresses in the surrounding concrete, resulting in spalling of the concrete cover and generally accelerates deterioration of the structure. As a result, frequent maintenance and repair works are needed to seal the cracks, especially for pavements and tunnel linings. It was estimated that 3.6 trillion dollars were needed for the maintenance and repairs of civil infrastructure from 2016 to 2020 in U.S [3].

Extensive researches have been conducted on the self-healing phenomenon in concrete. Concrete has been discovered to have the potential of sealing cracks by itself in the 1830s; it was observed that the

microcracks in a bridge in Amsterdam were sealed with some white crystal residues under moist environment [4]. Such a phenomenon is referred to as "self-sealing" or more often "self-healing". Such self-healing phenomenon in concrete is a result of the combined effects of multiple mechanisms which include the precipitation of CaCO<sub>3</sub> and continue hydration of unhydrated cement particles in water bearing cracks [5]. For concrete containing mineral admixtures, such as fly ash, continued pozzolanic reactions also contribute to the self-healing process [6–10].

Although concrete has shown self-healing ability, it is rarely observed in concrete infrastructures. This is because the crack width is a critical factor for the occurrence of self-healing phenomenon. In previous studies, it was found that cracks with width below 50  $\mu m$  could be fully healed, while incomplete healing was usually observed when the crack is wider than 100  $\mu m$  although self-healing products could be found [6,7,11–13]. Nevertheless, cracks in normal concrete often reach millimeters in width even when restrained by steel rebar. Controlling the crack width in concrete is highly desirable to ensure robust self-healing ability.

Engineered cementitious composite (ECC) is a high-performance fiber reinforced cementitious composites (HPFRCC) designed based on micro-mechanics [14,15]. ECC suppresses brittle fracture by virtue of

E-mail addresses: zhangzg@cqu.edu.cn (Z. Zhang), qxz7311@gmail.com (Q. Zhang), vcli@umich.edu (V.C. Li).

<sup>\*</sup> Corresponding author.

<sup>\*\*</sup> Corresponding author.

its tensile strain hardening behavior and high strain capacity (3%–8%) [16–19]. In addition, the width of microcracks in ECC is typically below 60  $\mu$ m even when strained to several percent [20]. This intrinsic ability to controlling crack width slows water permeation and chloride diffusion into the interior of ECC [1,5,21]. Further, the tight crack width of ECC naturally results in good self-healing capability, thus enabling gains in the durability of ECC structures [10,21].

Over the past decade, much research has been carried out on the self-healing behavior of ECC. Yang and Li [12] found that the resonant frequency of crack-damaged ECC could recover to its initial value after wet-dry cycles. Under a hydraulic gradient, the water permeability of cracked-ECC was found to decrease gradually, a phenomenon that was attributed to self-healing [21,22]. Chloride diffusion coefficient through damaged ECC was also shown to recover due to self-healing [7,10]. Self-healing was observed in pre-cracked ECC specimens exposed to freezing-and-thawing cycles and marine environment [23,24]. A combination of C–S–H and CaCO<sub>3</sub> was normally found in the self-healing products in the healed cracks in ECC [11,25].

In ECC, self-healing is shown to recover transport as well as mechanical properties. Yang et al. [12] reported that the tensile ductility of self-healed ECC was retained after damaged by pre-straining up to 3%. Qian et al. [25,26] investigated the self-healing behavior of ECC and found that the deflection capacity and flexural stiffness of cracked-ECC regained by 100% and more than 40–60%, respectively, when compared with virgin specimens. Notable recovery of ECC tensile properties was also observed in the natural environment. ECC specimens pre-loaded to 1% tensile strain showed first cracking strength and stiffness recovery up to 100% when stored outdoors for 6 months in Ann Arbor, Michigan state in the US [27].

The self-healing products that fill up the crack volume in ECC were found to be influenced by the mix composition and curing condition. For example, researchers [6,28] have discovered that the addition of supplementary cementitious materials or hydrated lime in ECC resulted in better tensile stiffness and strength recovery due to their pozzolanic effects. Also, in a previous study conducted by the authors [29], exposure to calcium hydroxide solution and hot water were demonstrated to improve the level and rate of tensile stiffness recovery (recovered to 47% and 61%, respectively, as compared with that of 35% under water curing) in pre-damaged ECC.

To date, most previous research on self-healing induced mechanical property recovery of ECC were conducted at the composite scale. Recently, Ma et al. [30] developed an analytic model aimed at linking the meso-scale single crack level self-healing behavior to macro-scale composite level stiffness recovery. They concluded that smaller crack width in ECC is preferred for higher stiffness recovery level. Qiu et al. [31] suggested that the self-healing phenomenon in ECC was likely a result of fiber/matrix interfacial bond restoration. Despite these studies, there remains a need to explore the micromechanics behind mechanical property recovery in ECC. To enrich the knowledge of self-healing behavior in ECC, the present paper aims at a systematic multi-scale experimental investigation to further reveal the mechanisms of mechanical property recovery of self-healed ECC. At the macro-scale, the tensile and flexural property recoveries of pre-damaged ECC were experimentally assessed. At the meso-scale, the influence of self-healing on the fiber bridging behavior across a single crack plane was characterized via single crack tests. At micro-scale, the recovery of fiber/ matrix properties due to self-healing was studied via single fiber pullout studies.

#### 2. Micromechanics-based ECC design theory

Instead of the conventional trial-and-error material design method, ECC mixtures are designed under the guidance of micro-mechanics theory. Micromechanics-based ECC design theory links the mechanical performances of ECC at the macro-scale (i.e. tensile strength, tensile ductility, crack widths, etc.) to meso-scale properties (i.e. fiber bridging

behavior) and then to properties at micro-scale (i.e. fiber stiffness, fiber strength, fiber/matrix interfacial bond, matrix toughness, flaw size, etc.). The design theory has been extensively used to guide the design of new functional ECC mixtures and to understand the behavior of ECC under various loading and environmental conditions. In this paper, it is used to assist in the understanding of the self-healing behavior of ECC at multiple length scales.

To achieve the unique behavior of multiple cracking, strain-hardening behavior, and self-controlled tight crack widths, two criteria need to be satisfied [14,32]: the energy-based criteria and the strength based criteria as shown in equations (1) and (2).

Energy – based criterion: 
$$J_{tip} \le \sigma_0 \delta_0 - \int_0^{\delta_0} \sigma(\delta) d\delta \equiv J'_b$$
 (1)

Strength – based criterion: 
$$\sigma_0 > \sigma_{cs}$$
 (2)

where  $J_{lip}$  is the energy needed for the propagation of a crack in matrix;  $J'_b$  is the fiber bridging complementary energy across a crack plane;  $\sigma_0$  is the maximum fiber bridging stress corresponding to the critical crack opening  $\delta_0$  across a crack; and  $\sigma_{cs}$  is the cracking strength of the matrix under tension.

The energy criterion described in Equation (1) states that the energy balance required by the crack extension, that is the crack tip toughness  $(J_{tip})$  must not exceed the complimentary fiber bridging energy  $(J'_b)$ . This ensures the steady-state flat crack propagation in ECC; otherwise, a typical Griffith crack will occur, resulting in localized cracking.  $J_{tip}$  is primarily a matrix property that can be estimated as the square of matrix fracture toughness  $(K_m)$  divided by matrix elastic modulus  $(E_m)$ . The complimentary fiber bridging energy  $(J'_b)$  can be calculated from the fiber bridging stress-crack opening  $(\sigma - \delta)$  relationship (the right hand side of equation (1)) as illustrated in Fig. 1 [14,32]. The strength criterion states that the cracking strength of matrix  $(\sigma_{cs})$  must be less than the minimum fiber bridging strength  $(\sigma_o)$  of all cross-sections. Failure to meet either criterion will lead to a single localized fracture instead of multiple cracking behaviors in ECC.

The  $\sigma$ - $\delta$  curve can be directly measured via single crack tests (detailed in section 3.2.3). Alternatively, since it is governed by the interfacial interactions between fibers and cementitious matrix at microscale, it can also be determined by single fiber pull-out tests and a scale linking model. Li and co-workers [33–35] developed an analytical model to represent the behavior of a single fiber being pull-out from surrounding matrix and a scale-linking model to aggregate the single fiber behavior to obtain the average  $\sigma$ - $\delta$  relationship. The parameters used in the single fiber pullout model include the fiber/matrix interfacial chemical bond ( $G_d$ ) and frictional stress ( $\tau_0$ ), and slip-hardening coefficient ( $\beta$ ). These parameters can be obtained from single fiber pull-

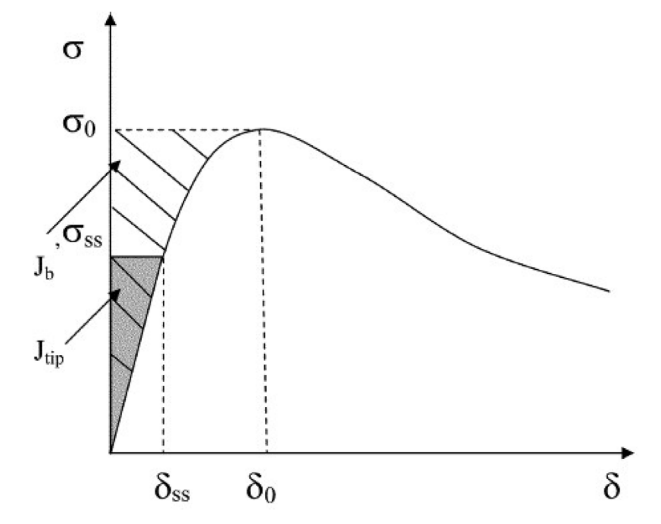


**Fig. 1.** The typical fiber bridging stress-crack opening  $(\sigma-\delta)$  relationship.

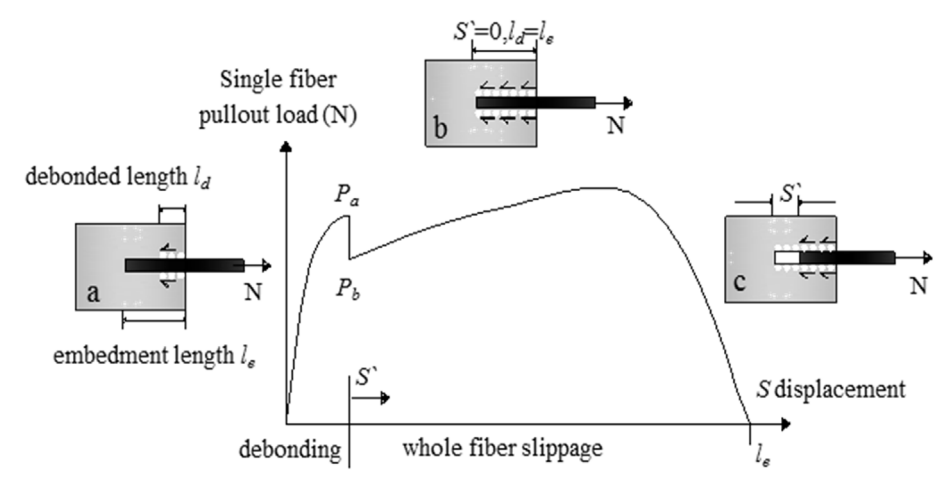


Fig. 2. The typical pull-out process of single PVA fiber [35].

out tests.

Fig. 2 shows a typical load-displacement curve of a single poly-vinyl alcohol (PVA) fiber being pulled out from the cementitious matrix [36]. At the first stage, the PVA fiber embedded in the matrix undergoes a debonding process, which leads to a load increase up to  $P_a$ . Then the load experiences a sudden drop from  $P_a$  to  $P_b$  due to the loss of chemical bond. This denotes the end of the debonding process and the starting of fiber slippage. During fiber slippage process, the load begins to increase again due to the slip-hardening behavior of PVA fibers in the cementitious matrix until the fibers being gradually pulled out or fracture, whichever happens first. The chemical bond ( $G_d$ ) and frictional bond ( $G_d$ ) on the fiber/matrix interface can be calculated from the values of  $G_d$  and  $G_d$  and  $G_d$  as follows:

$$Gd = \frac{2(Pa - Pb)^2}{\pi^2 E_f d_f^3}$$
 (3)

$$\tau = \frac{Pb}{\pi d_f l_e} \tag{4}$$

where  $E_f$  is the modulus of fiber,  $d_f$  is the diameter of fiber,  $l_e$  is the embedded length of fiber in matrix. The slip-hardening coefficient (β) can also be determined from the shape of the pull-out curve after the first load drop. These parameters can then be used in the analytic model to obtain the σ-δ relationship.

# 3. Experimental program

#### 3.1. ECC mixture and specimen preparation

Type I Portland cement, class F fly ash, silica sand with average grain size of 110  $\mu m$ , water, polycarboxylate-based high range water reducer (HRWR) and PVA fiber were used to prepare the ECC specimens. Table 1 presents the ECC mixture proportion, which was widely used in previous studies [22,37]. The chemical compositions and physical properties of fly ash are summarized in Table 2.

The mixing process followed a standard ECC mix procedure which could be found in previous literature [38]. After mixing, the fresh ECC paste was cast into molds and covered with plastic sheets for 1 day before demolding. Then all ECC specimens were cured in air at room

**Table 1**The mixture proportions of ECC.

Cement (c)	Fly ash (FA/c)	Silica sand (s/cm)	Water (w/cm)	HRWR (WR/c)	PVA fiber (by volume)
1.0	2.2	0.36	0.25	0.03	2%

 Table 2

 Chemical compositions and physical properties of fly ash.

SiO <sub>2</sub> , %	44.09	Na <sub>2</sub> O, %	0.99
Al <sub>2</sub> O <sub>3</sub> , %	23.21	K <sub>2</sub> O, %	1.63
Fe <sub>2</sub> O <sub>3</sub> , %	8.39	Total alkalis, %	1.86
Sum, %	75.69	Loss on ignition, %	0.95
CaO, %	14.04	Strength activity index with Portland cement at 28 days, % of control	92
MgO, %	3.04	Fineness, % retained on #325	16.85
SO <sub>3</sub> , %	1.46	Specific gravity (g/cm3)	2.45

temperature of 20  $\,\pm\,$  3 °C and relative humidity (RH) of 40  $\,\pm\,$  5% until testing at 28 days.

#### 3.2. Experimental procedures

In this study, tensile tests, flexural tests, single crack tests, and single fiber pull-out tests were conducted to study the self-healing behavior of ECC at multiple length scales. Additionally, digital optical microscope was also used to observe the healing products within the crack.

#### 3.2.1. Tensile test

Uniaxial tensile test on dog-bone shaped specimens was conducted in this study to directly assess the tensile property recovery of selfhealed ECC specimens at macro-scale. The adoption of dog-bone specimens allows cracks to form within the gauge length due to the smaller cross-sectional area than the end regions. The dimensions of gauge length zone in specimens are 80 mm  $(length) \times 30 \, mm$ (width) × 13 mm (thickness). The ECC specimens were tested under displacement control at a loading rate of 0.5 mm/min. The tensile strain was measured based on the change in gauge length as measured by two LVDTs attached to the specimen. The detailed test set-up could be found in Ref. [39].

The average tensile strain capacity of the ECC mixture used in this study was measured to be 4.4% in a previous study [22]. Therefore, in this study, the ECC tensile specimens were pre-loaded at 28 days to 4 different strain levels: 1%, 2%, 3%, and 4%. This ensures that the specimens were micro-crack damaged without fracture localization. After pre-loading, the pre-damaged ECC specimens underwent 10 wetdry self-healing cycles, where one cycle is composed of immersion in water for 24 h and drying in air for another 24 h. After 10 wetdry cycles, the pre-damaged ECC specimens were re-loaded under tension until failure. Virgin ECC specimens (without pre-damage) was tested at 28 days and used as a reference to determine the level of mechanical properties recovery of self-healed specimens. A control group of pre-cracked specimens without wet-dry cycles was also re-loaded at the

same test age as that of self-healed specimens for comparison purpose.

#### 3.2.2. Flexural performance

Four-point bending test was adopted to assess the level of flexural performance recovery of self-healed ECC. The dimension of the beam specimen for four-point bending test is 305 mm (length)  $\times$  76 mm (width)  $\times$  38 mm (height). The full span length for this test is 300 mm with a middle span of 100 mm. The loading rate in this test is 0.5 mm/min. The deflection of specimens was measured at the loading points, as recorded by instrument stroke during testing.

During the test, the flexural specimens were pre-loaded to a loading-point deflection of 3 mm to initiate crack damage at the bottom face of the specimens, while the deflection capacity of the ECC used in this study is about 8 mm as reported in Ref. [37]. Then the pre-cracked beam specimens underwent the wet-dry cycles. After 10 wet-dry cycles, the healed specimens were re-loaded via four-point bending test until failure. The recovery of flexural properties of self-healed ECC specimens, including the initial stiffness, flexural strength, and deflection capacity, were compared with the control specimens (without pre-damage) that are tested under monotonic loading up to failure at 28 days to evaluate its self-healing effectiveness.

#### 3.2.3. Single-crack tensile test

Following Pereira et al. [40], notched dog-bone specimens as shown in Fig. 3 were used to directly measure the fiber bridging stress vs. crack opening  $(\sigma\text{-}\delta)$  relationship and its recovery after self-healing. A continuous notch was made all around the specimen at mid-length of the dogbone specimen (dimension of the dogbone specimen is as described in section 3.2.1). The size of the notch is shown in Fig. 3. Uniaxial tensile load at the rate of 0.5 mm/min was applied to the specimen to induce cracking at the notch location. Two LVDTs were placed at a gage length of 20 mm as shown to measure the crack opening. It should be noted that it is very difficult to form only a single crack in ECC due to the intrinsic high ductility of ECC, even with notches. Therefore, in this study, only 1% of PVA fibers were used to ensure the formation of only one single crack.

To assess the self-healing induced recovery of the fiber bridging behavior, six notched dogbone specimens were pre-loaded to form one single micro-crack at 28 curing days, and this pre-loading process was terminated when crack width reached around 50  $\mu m$ . After pre-loading, three specimens were exposed to 10 wet-dry self-healing cycles before re-loaded to failure, while the other three were exposed to air for 20 days (the same age of 10 wet-dry cycles) before re-loading as a comparison. A control group of three single crack specimens were tested under monotonic loading at 28 days.

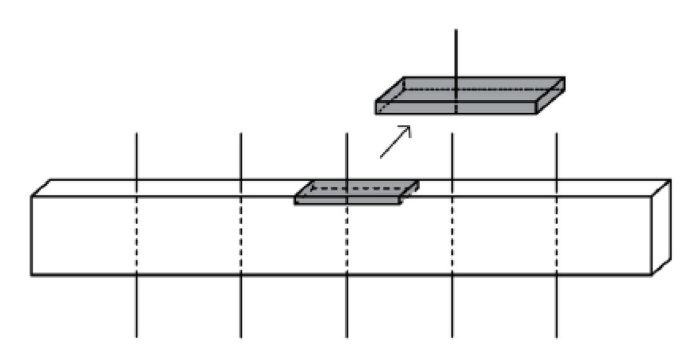


Fig. 4. Schematic diagram of sample preparation for single fiber pull-out test.

#### 3.2.4. Single fiber pull-out test

The single fiber pull-out test characterized the load-displacement relationship of a single fiber pulled-out from matrix. Single fiber pullout specimen consists of a single PVA fiber embedded in the ECC matrix (without fibers). During the test, the fiber was pulled out from the ECC matrix at a displacement rate of 0.5 mm/min and the load-displacement curve was recorded and used to characterize the fiber/matrix interfacial bond properties. The fiber embedment length in samples is around 1.0 mm. The samples preparation for this test is schematically illustrated in Fig. 4. The small embedment length is chosen to avoid premature rupture of the fiber and to ensure successful capture of the entire debonding and pullout process. The test set-up and procedures can be found in Refs. [41,42].

To characterize the effect of self-healing, a control group of six samples was tested at 28 curing days until rupture of the fiber to obtain the full single fiber pull-out curve which was used to calculate fiber/matrix interface properties of the ECC mixture. This provided a reference for follow-up tests on self-healed samples. A number of samples were pre-loaded to the end of debonding process (the test was aborted when a sudden load drop occurred), then the samples went through 10 wet-dry cycles before they were re-loaded to failure. In this manner, five re-loading curves were obtained successfully.

# 4. Results and discussions

## 4.1. Influence of self-healing on tensile performance of ECC

Table 3 summarizes the measured 28 days mechanical properties of the ECC mixture used in this study. The listed values were obtained based on the testing of four specimens. This provides a baseline for assessing the mechanical property recovery caused by self-healing. ECC shows a ductile behavior under tension and flexure with a measured

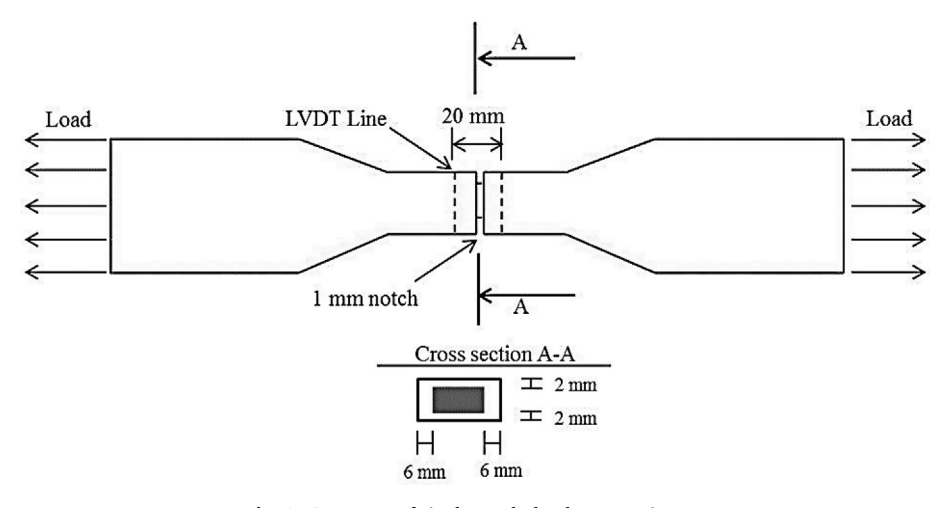


Fig. 3. Geometry of single-crack dog-bone specimens.

**Table 3**Mechanical properties of ECC.

Tensile strength	Strain Capacity	Flexural strength	Deflection capacity	Compressive strength
5.8 ± 0.5 MPa	4.4 ± 0.3%	12.2 ± 0.7 MPa	7.9 ± 0.2 mm	45.8 ± 2.5 MPa

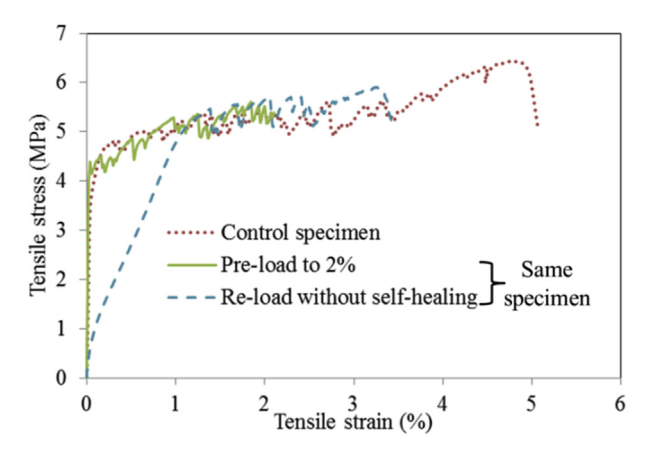
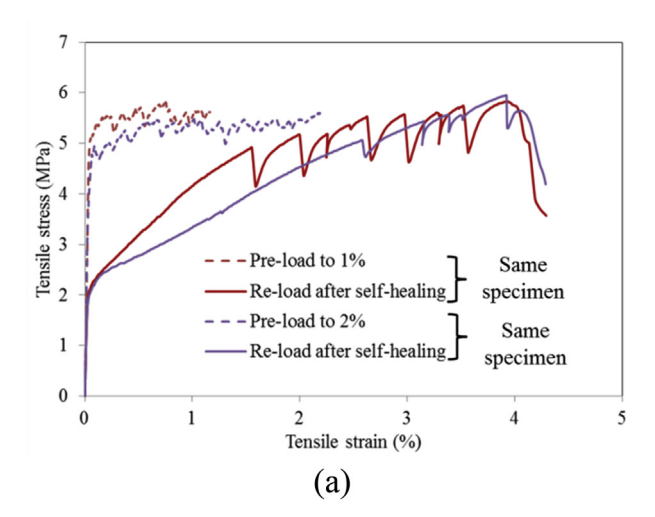


Fig. 5. Tensile stress-strain relationships of pre-load and re-load ECC specimen.

tensile strength of 5.8 MPa, tensile strain capacity of 4.4%, the flexural strength of 12.2 MPa and loading point flexural deflection capacity of 7.9 mm. The compressive strength of the mixture is also measured using cube samples with a dimension of  $50.8 \, \text{mm} \times 50.8 \, \text{mm} \times 50.8 \, \text{mm}$  according to ASTM C109 [43] and the test value is listed in Table 3.

Fig. 5 shows the representative tensile stress-strain curves of ECC specimen pre-loaded to 2% strain and then unloaded. This specimen was then reloaded without self-healing. The stress-strain relationship of a control specimen at 28 curing days measured under monotonic loading up to failure is also shown as a comparison. The stiffness of the re-loading curve, defined as the slope of the initial stress-strain curve, is substantially reduced as compared with that in pre-loading and control curves. This is due to the fact that at crack locations, the matrix has already cracked and only the partially debonded fibers were bridging the cracks and carrying the tensile loads during re-loading. Since fibers have a much lower volume (2%) and effective stiffness ( $V_t E_t$ ) than the uncracked matrix  $((1-V_f)E_m)$ , this leads to a much lower stiffness of the re-loading curve of the unhealed ECC specimens. Moreover, the tensile strain capacity of the re-loaded specimen (without self-healing) also decreases greatly in comparison with that from the monotonic test (control case) because part of the strain capacity has already been exhausted during pre-loading.

Fig. 6 shows the measured tensile stress-strain relationships of selfhealed specimens during re-loading. For comparison, the pre-loading curves are also plotted in the same figure. After 10 wet-dry cycles, specimens pre-loaded to all strain levels all showed a highly ductile strain-hardening behavior with tensile strain capacity around 4%, which was very close to that of the uncracked specimens (4.4%). It can also be seen from the re-loading curves of the self-healed samples that the stiffness of ECC had an evident rebound, which is attributed to the combined effects of micro-cracks healing and the enhanced stiffness of bulk matrix caused by continuous hydration of unhydrated cement. Meanwhile, the first cracking strength, defined as the stress corresponds to the end point of the initial linear stage, recovered to approximately 2 MPa for samples pre-loaded to all strain levels. However, for selfhealed specimens, after first cracking, the tensile stress increases smoothly as the tensile strain develops, which is different from the typical fluctuating stress-strain curves caused by stress drops at the occurrence of micro-cracks. This phenomenon suggests that, during reloading, the healed micro-cracks in ECC opened first causing little disturbance in stress. This also explains the lower stresses compared to



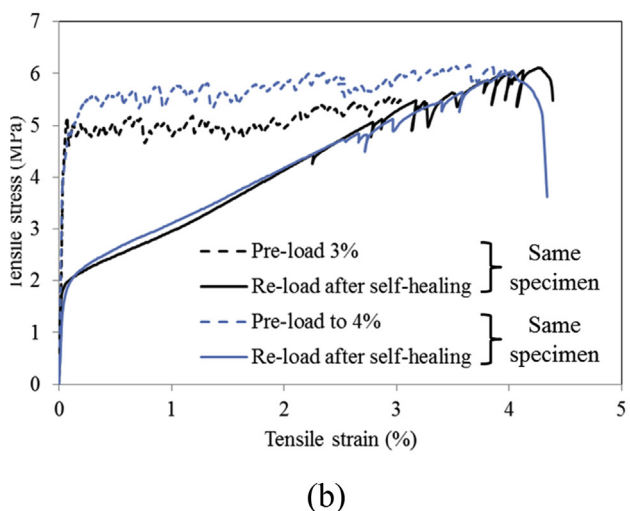


Fig. 6. Tensile strain-stress curves of pre-loaded specimens after self-healing.

the pre-loading curve at this stage. Towards the later stage of reloading, stress-strain relationship returns to the fluctuating shape, indicating the generation of new micro-cracks in ECCs. It should be noted that not all pre-cracks re-opened, which will be discussed later.

Fig. 7 illustrates the recovery percentage of tensile properties of ECC induced by self-healing. The recovery percentage is defined as the ratio between measured tensile properties of self-healed ECC specimens to that of the control specimens tested under monotonic loading at 28 days. The residue tensile properties of unhealed specimens with preloaded to 2% is also given in Fig. 7. It shows that, as compared with the unhealed case, the stiffness, first cracking strength, and strain capacity of ECC have all recovered notably due to self-healing. The recovery level of stiffness reaches 92% for the ECC specimens pre-loaded to 1% strain, and tends to decrease as the pre-damage level increases. Nevertheless, even when pre-loaded to 4%, it still achieves about 60% recovery of stiffness after 10 wet-dry cycles. The strain capacity of ECC recovers to above 90% of the original value (tested at 28 days) after self-healing for specimens pre-loaded to all strain levels. In terms of first cracking strength, the recovery percentage ranges from 40% to 50% for specimens at four different pre-damaged levels. The relatively lower

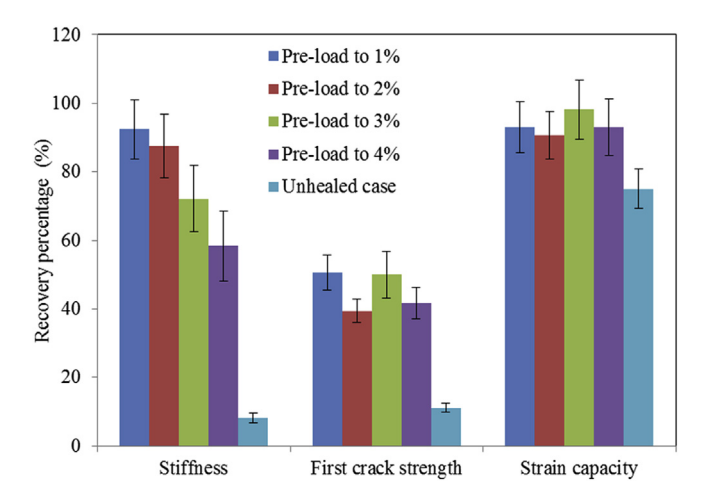


Fig. 7. The recovery percentage of ECC's tensile performance.

recovery percentage in first cracking strength is due to the variation of self-healing efficiency at different micro-crack sites, as it is governed by the weakest micro-crack plane. On the other hand, the strength of self-healing products might be relatively lower than that of matrix, which also leads to the lower recovery of first cracking strength. However, it has been reported that the first cracking strength in pre-damaged ECC could restore over its original value if the specimens were to go through longer self-healing cycles [27].

Fig. 8 presents the crack pattern of self-healed ECC specimens after re-loading. It shows that both healed micro-cracks in ECC re-opened and new cracks formed. It can be seen from the right figure that a small number of healed micro-cracks in ECC remains closed even after reloading. Both the re-opening of healed cracks and formation of new cracks in ECC specimens contribute to the high strain capacity of self-healed ECC during re-loading. This may also explain that all specimens, despite their pre-damage levels, achieved very similar strain capacity during re-loading.

Table 4 lists the crack information including the number of cracks and average crack width of ECC specimens during pre-loading and reloading. As listed in Table 4, the number of cracks in the pre-loaded ECC specimen increases while the average crack width maintains around 30  $\mu m$  as the pre-loaded strain level increases. As has been illustrated in Table 4, the number of cracks in ECC after reloading is higher than that of the pre-loaded ones.

Fig. 9 displays the formation of self-healing products in microcracks as a function of the number of wet-dry cycles. It shows in Fig.  $9(a) \sim (c)$  that the self-healing products form at the surfaces of the crack and grows towards the middle of the crack until the crack is fully sealed. Additionally, the fibers bridging the crack also provide nucleation sites for self-healing products as illustrated in Fig. 9(d).

**Table 4**Crack information in ECC specimen.

Preloaded strain level	1%	2%	3%	4%
Average crack width (pre-load)	26 μm	31 μm	28 μm	34 μm
Number of cracks (pre-load)	15	28	37	41
Number of cracks (re-load)	56	56	47	51

#### 4.2. Influence of self-healing on flexural performance of ECC

The flexural stress-load point displacement curves of the self-healed ECC measured during pre-loading and re-loading are shown in Fig. 10. Those of unhealed specimen during re-loading and that of un-damaged control specimens tested at 28 days are also shown as references.

It can be seen that the pre-cracked specimen without self-healing had a very distinct deterioration in flexural stiffness, deflection capacity and flexural strength as compared with the control specimen. The flexural stiffness and deflection capacity are defined as the slope of the initial elastic stage and the load point displacement corresponding to the maximum flexural stress, respectively. In contrast, for self-healed specimens, it shows remarkable recovery of flexural stiffness, flexural strength, and deflection capacity.

Similar to the tensile stress-strain curves, the flexural stress-deflection curve of self-healed specimen also shows an initial smooth portion followed by the typically fluctuating portion at later stage, while, there is no fluctuating portion observed for unhealed specimen. This indicates that the healed cracks typically re-open first and then new cracks form at later stage, while, in the case of unhealed one, the stress fluctuation and new cracks were not observed. This observation suggests that the fiber bridging capacity ( $\sigma_0$ ) across the existing micro-cracks is restored due to the self-healing phenomena, and results in increased margin between  $\sigma_0$  and  $\sigma_{cs}$  as mentioned in equation (2), therefore allows the formation of more new cracks in ECC, and consequently higher deflection capacity in self-healed beam specimens. The restoration of fiber bridging capacity was also confirmed in section 4.3.

Fig. 11 presents the residue percentage of flexural properties of predamaged ECC specimens with and without self-healing normalized by those of control specimens tested under monotonic loadings at 28 days. It could be clearly seen that the flexural stiffness, deflection capacity, and flexural strength of self-healed ECC is higher than that of un-healed one. The effect of self-healing on deflection capacity is most significant since it recovers to 83.5% that of control case as compared with 43% for un-healed specimen. On the other hand, due to the effects of self-healing, the flexural stiffness and strength of pre-damaged ECCs recover to 42% and 100% of those of control specimens, while the residue percentage of non-healed specimens are 27% and 90% of those of control ones, respectively. 100% recovery of strength observed in ECCs is rarely observed in normal self-healing concrete.

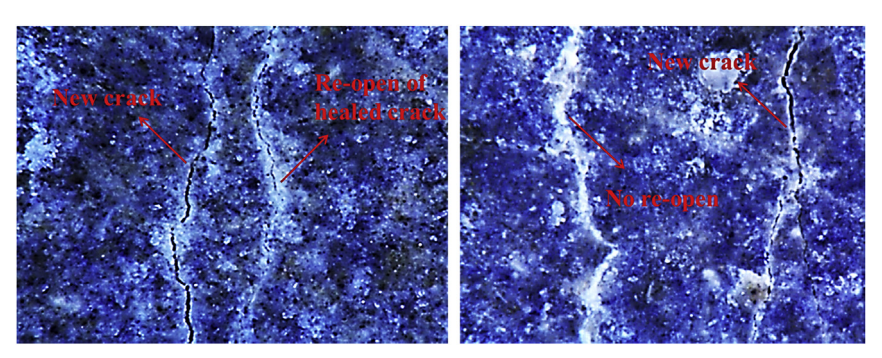


Fig. 8. Crack pattern of self-healed ECC after reloading.

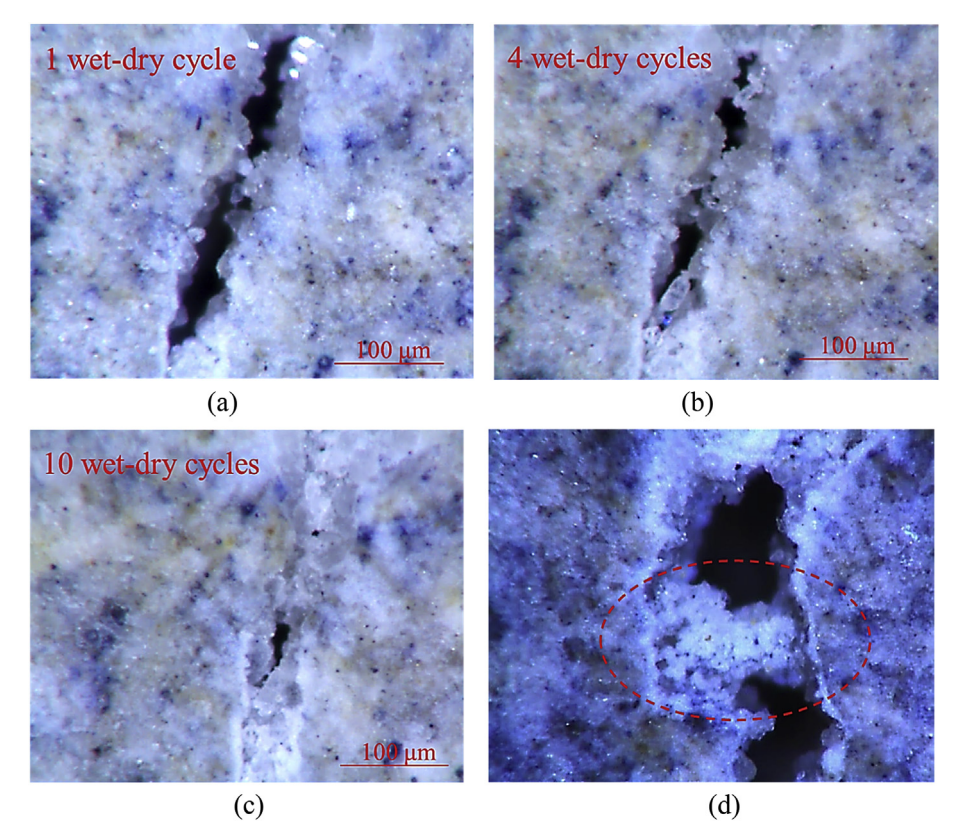


Fig. 9. Self-healing products in crack at different wet-dry cycles (observed by 200x light micro-scopes).

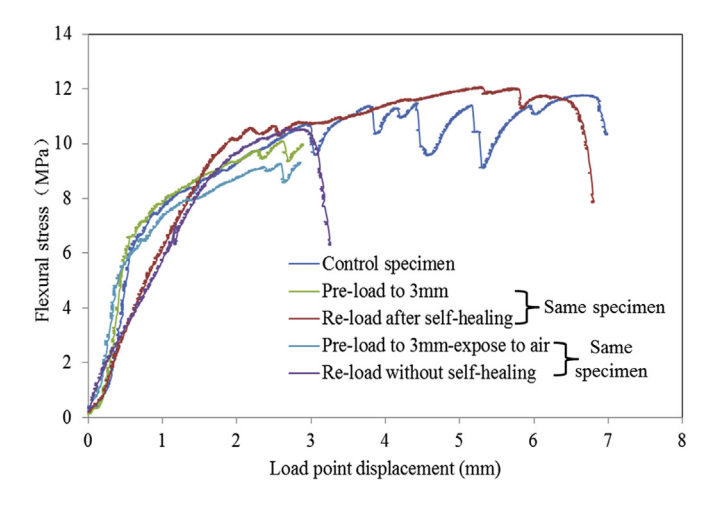


Fig. 10. The flexural behavior of pre-cracked ECC after self-healing.

#### 4.3. Influence of self-healing on fiber bridging behavior of ECC

The representative fiber bridging stress-crack opening displacement curves of notched specimens are presented in Fig. 12. Table 5 summarizes the value of the maximum fiber bridging stress across one single crack in ECC by averaging the measurements for three specimens. The pre-crack and re-loading curves plotted in the same color in Fig. 12 are from the same specimen. It could be seen from Fig. 12 and Table 5 that the maximum bridging stress of the pre-cracked specimens without self-healing dramatically dropped to 2.71 MPa when compared with the control case (3.59 MPa), and recovered to 3.52 MPa for the self-healed specimen, almost the same as that of the control. It demonstrates that the self-healing phenomenon in ECC leads to a recovery of the fiber bridging capacity across the cracks, which explains the

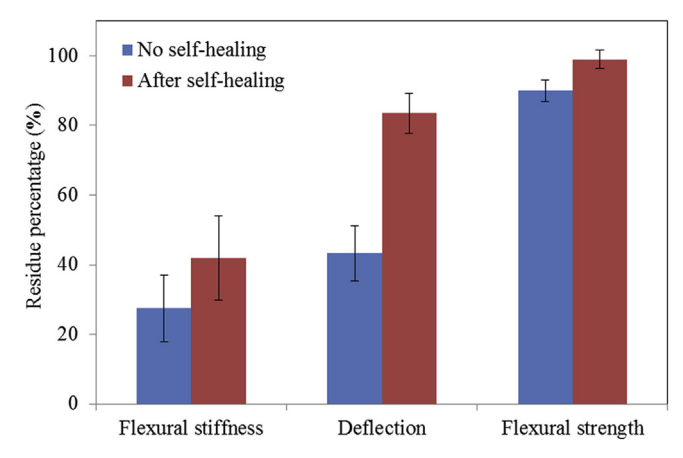


Fig. 11. The flexural performance self-healed recovery level of ECC.

evident rebound in tensile/flexural strength of ECC at the macroscale as the ultimate tensile and flexural strength of ECC is mainly determined by the fiber bridging strength at the failure crack plane. The regain of fiber bridging strength leads to a recovery of maximum fiber bridging stress ( $\sigma_0$ ) and complementary energy ( $J_b$ ), and subsequently restores the strain hardening potentials  $PSH_E$  (=  $J_b/J_{tip}$ ) and  $PSH_s$  (=  $\sigma_0/\sigma_{cs}$ ) in the self-healed ECC specimens [34], ultimately resulting in the recovery of tensile and flexural ductility.

It is hypothesized that the possible reasons for the recovery of fiber bridging capacity in ECC are bulk matrix strengthening and matrix/fiber interface recovery. To further investigate the underlying mechanism, an environmental scanning electric microscope (ESEM) was used to observe the side of the self-healed crack in ECC, as shown in Fig. 13. This sample was fractured by hand to keep its original morphology inside crack and avoid the damage to the self-healing product that might be introduced by saw-cutting. It could be seen from Fig. 13

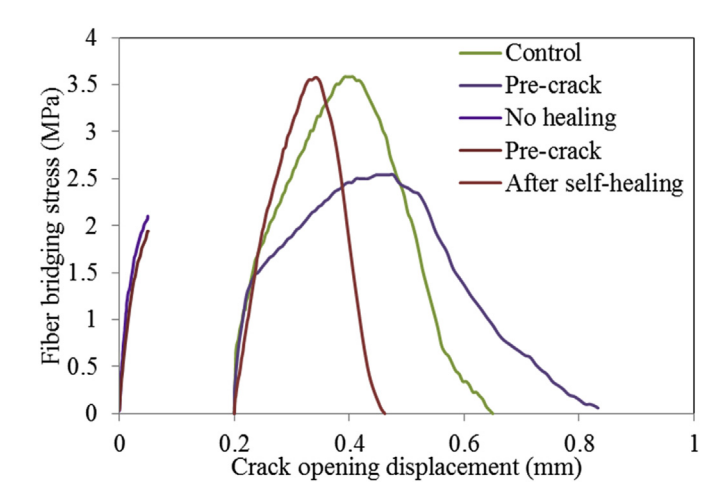


Fig. 12. Fiber bridging performance of ECCs.

**Table 5**Fiber bridging capacity of ECC with 1% fiber volume.

	Control case	No healing	After self-healing
Maximum fiber bridging stress	3.59 ± 0.07 MPa	2.71 ± 0.43 MPa	3.52 ± 0.08 MPa

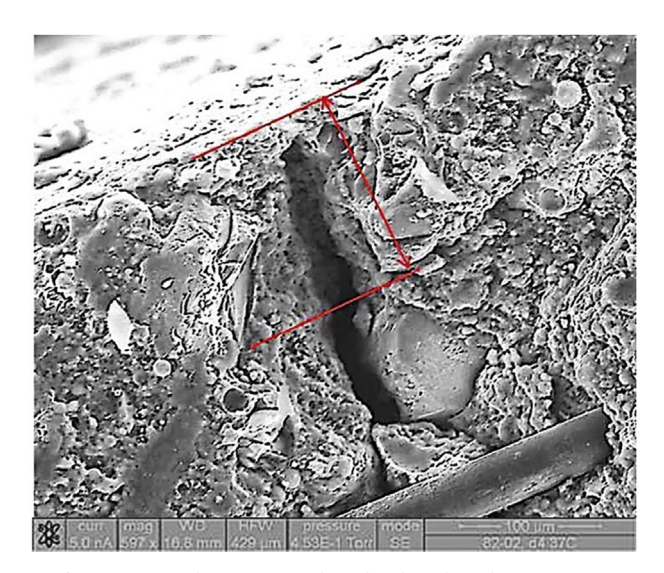


Fig. 13. ESEM observation at the side-edge of crack area in ECC.

that the self-healing products are found only within around  $100\,\mu m$  depth from the surface of the sample. This is clear evidence that the self-healing product does not fully fill the crack volume, consistent with that reported by Fan and Li [44]. Accordingly, the tensile/flexural stiffness and strength recovery are not solely caused by the self-healing products in the crack volume. Rather, the recovery of the matrix/fiber interface plays an important role, since the interface properties govern the fiber-bridging behavior and therefore the mechanical performance of ECC in the strain-hardening stage. Additionally, the self-healing products (attached on fiber as shown in Fig. 9 (d)) together with PVA fiber could be considered a micro-composite, with a relatively higher stiffness than the fiber itself, thereby contributing to the recovery of stiffness and first cracking strength of ECC to some degrees.

# 4.4. Influence of self-healing on matrix/fiber interface properties

The typical test curves obtained from single fiber pull-out test of

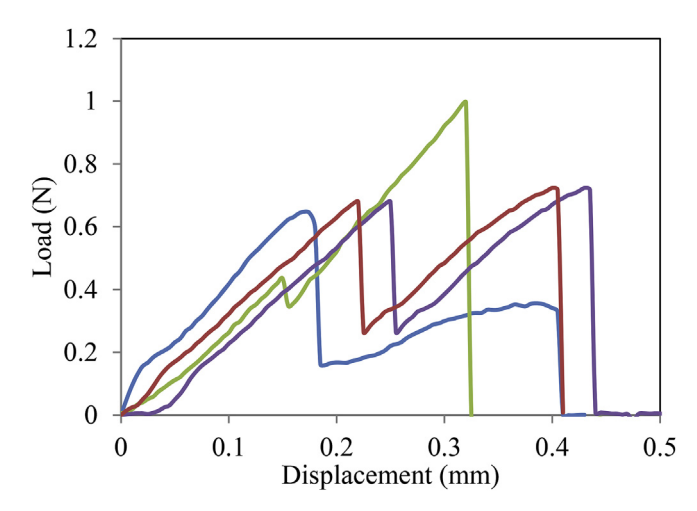


Fig. 14. Typical single fiber pull-out curves of PVA fiber in ECC matrix.

control specimens are displayed in Fig. 14. As shown in Fig. 14, the load increases during the initial fiber debonding stage. After that, a sudden load drop appears that signifies the end of the fiber debonding process. The drop is caused by complete loss of chemical bond between the fibers and the cementitious matrix. After debonding and during the pull-out process, the interfacial bond is primarily frictional. The frictional stress can be calculated using the load immediately following the load-drop and the embedment length of the fiber. During the pull-out process, the load continues to increase due to a slip-hardening phenomenon until the fiber is completely pulled out or ruptures.

Fig. 15 presents the re-loading curves of pre-loaded single fiber specimens after undergoing self-healing process. The pre-loading curves are also included. Curves in the same color are from the same sample. In the re-loading curves, there is no sudden load-drop, which indicates that the chemical bond between debonded PVA fiber and surrounding matrix does not recover; as a result, the chemical bond  $(G_d)$  value for the self-healed sample is zero. As is known, the interfacial chemical bond mainly attributes to the buildup of Ca(OH)<sub>2</sub> layer in the interfacial transition zone (ITZ) [45,46], in the case of our self-healing experiment, the OH concentration is likely to be low due to the small sample being immersed in large volume of water, thus hindering the formation of Ca (OH)2, and in turn there was no notable recovery of chemical bond even after 10 self-healing cycles. On the other hand, the load shows a little jitter after the initial smooth increase stage. Based on the hundreds of test experiences, the curve normally develops smoothly during frictional debonding process as shown in Fig. 15. Therefore, the first jitter point (indicated by the red arrows) is considered to be the moment that the full fiber starts to slip; hence the interface frictional bond strength  $(\tau_0)$  is calculated based on the load value corresponding to this point.

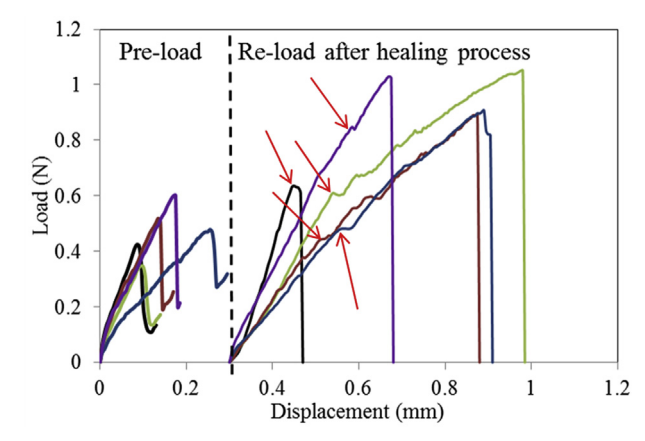


Fig. 15. The pre-load and re-load single fiber pull-out curves after self-healing.

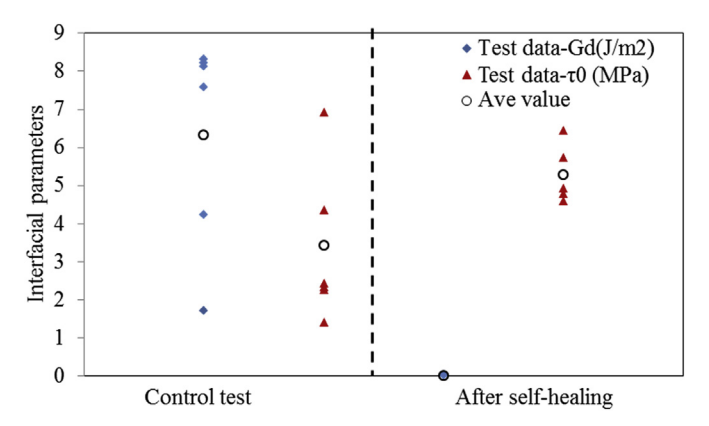


Fig. 16. Interface parameters from single fiber pull-out test.

During pre-loading process, the test was stopped immediately after the appearance of sudden load-drop signifying complete debonding. At this moment, the fiber just started to slip. It is assumed that the change of embedded length of fiber in matrix ( $l_e$ ) is negligible. Hence the  $l_e$  in Equation (4) retains its original value when calculating the  $\tau_0$  value after self-healing.

Fig. 16 exhibits the fiber/matrix interface parameters obtained from single fiber pull-out test. Compared with the value from control test under monotonic loading, the  $G_d$  value approaches zero for the preloaded sample even after the self-healing process, while the frictional stress  $(\tau_0)$  increases due to self-healing. As the frictional bond strength  $(\tau_0)$  has a direct relation to the compactness and stiffness of interfacial transition zone (ITZ) [47], it is hypothesized that healing products might be generated in the tunnel crack space induced by the debonding process, thereby increasing the compactness of the ITZ, and sequentially higher  $\tau_0$  value. SEM image at the exit point between PVA fiber and matrix (Fig. 17 (a)) reveals a gap between the fiber and matrix after debonding. After healing, however, crystal-like products are found in this gap (Fig. 17 (b)) which may support the aforementioned hypothesis.

To understand the mechanical property recovery of self-healed ECC from a micromechanical point of view, the fiber bridging stress-crack opening  $(\sigma-\delta)$  relationship (Fig. 18) was derived based on the measured interface parameters of self-healed specimens and micromechanical model of ECC [33]. The self-healed  $(\sigma-\delta)$  curve in Fig. 18 is computed based on the assumption that all the PVA fibers across the crack has completely debonded and not yet ruptured or pulled-out, and the interface is recovered due to self-healing process. It is a very conservative assumption because not all fibers have debonded and the residue interfacial chemical bond in the partial debonded fibers contributes to the fiber bridging capacity. It could be seen from Fig. 18 that, for the self-healed specimens, the maximum fiber bridging stress has increased in comparison with the control case. This is a direct result of

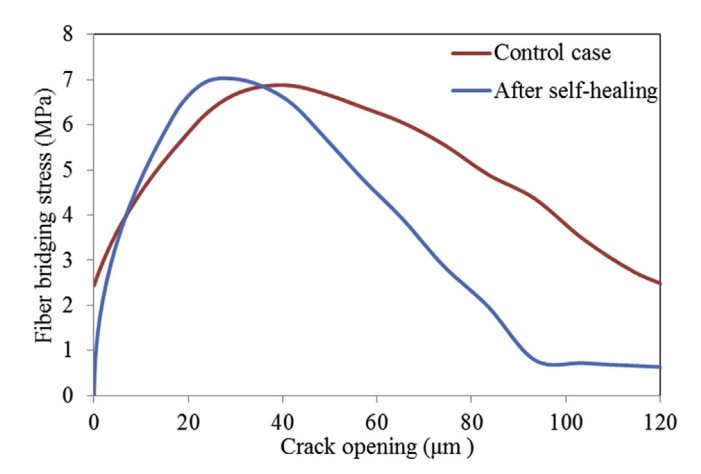


Fig. 18. Fiber bridging stress-crack opening relationships.

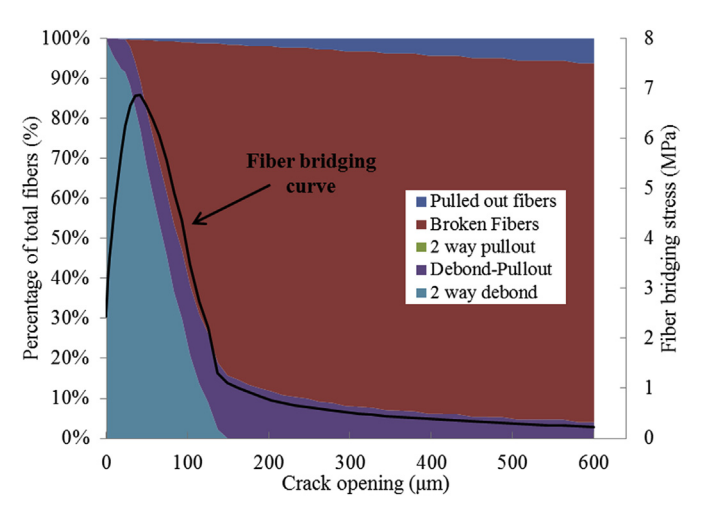


Fig. 19. Fiber status as the crack opening evolves.

the increase of  $\tau_0$  value despite the loss of chemical bond and could explain the tensile/flexural strength of ECC recovery after self-healing.

Fig. 19 illustrates the fiber status as the crack opening develop, computed based on ECC micromechanical model using fiber/matrix interfacial properties obtained from single fiber pullout tests of control specimens. At the critical crack opening of 42  $\mu m$  corresponding to the maximum fiber bridging stress, most fibers (76.8%) remain in the debonding process while 12.4% of fibers are in debonded-pullout status, 0.3% are pulled-out, and 10.5% are ruptured. This explains why ECC can retain substantial tensile/flexural strength at the composite scale level even after being pre-cracking without self-healing. Self-healing induces further improvement at matrix/fiber interface, resulting in the

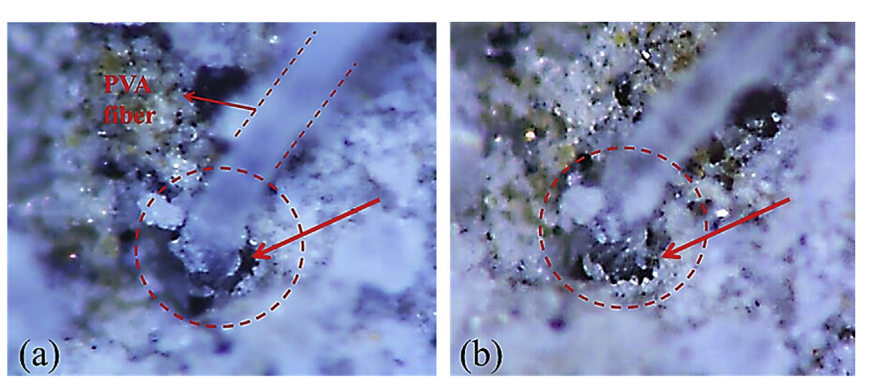


Fig. 17. Image observation of fiber/matrix exiting point by microscope (200 times).

recovery of tensile/flexural strength of ECC, and consequently restoration of composite ductility.

#### 5. Conclusions

In this paper, the influence of self-healing behavior on the mechanical properties of ECC was investigated at multiple length scales. The following conclusions can be drawn:

- At the macro-scale, the self-healing phenomenon resulted in a significant recovery in tensile/flexural stiffness, strain/deflection capacity, and strength of pre-damaged ECC.
- 2. At the meso scale, the maximum fiber bridging stress in self-healed ECC was found to restore to almost the same level (98%) as that of the undamaged samples, whereas a substantial reduction in bridging capacity is observed in un-healed pre-damaged samples. The ESEM observation suggested that the recovery in mechanical properties of ECC after self-healing process is associated with the recovery of the fiber/matrix interface properties. Partial recovery (~50%) of the matrix strength associated with rehealed chemical product growth connecting the crack faces was observed.
- 3. At the micro scale, single fiber pullout tests revealed that the interface chemical bond  $(G_d)$  of completely debonded fiber was not restored under the wet-dry cycle condition used in this study. However, the frictional bond  $(\tau_0)$  restored to a value even higher than that of the undamaged control samples, leading to the significant recovery of the fiber bridging capacity at the meso scale, and subsequently recovery of the mechanical properties at the macro-scale.

## Acknowledgements

The authors would like to graciously thank the National Natural Science Foundation of China (Grant No. 51708061), and 111 Project of China (Grant No. B18062), and the Science and Technology Research Program of Chongqing Municipal Education Commission (Grant No. KJQN201800126), and the Fundamental Research Funds for the Central Universities (Grant No. 2019CDXYTM0032, 2018CDJSK04XK09) for the financial support of this work. This research is partially supported by the National Science Foundation of USA (Grant No. CMMI 1634694) and by the James R. Rice Professorship at the University of Michigan.

#### References

- [1] K. Wang, D.C. Jansen, P.S. Shah, A.F. Karr, et al., Permeability study of cracked concrete, Cement Concr. Res. 27 (1997) 381–393.
- [2] H. Reinhardt, M. Jooss, Permeability and self-healing of cracked concrete as a function of temperature and crack width, Cement Concr. Res. 33 (7) (2003) 981–985.
- [3] ASCE, Report Card for America's Infrastructure. 2013, American Society of Civil Engineers, Washington DC, 2013.
- [4] K. Van Breugel, Is there a market for self-healing cement-based materials, Proceedings of the First International Conference on Self-Healing Materials, 2007.
- [5] C. Edvardsen, Water permeability and autogenous healing of cracks in concrete, Mater. J. 96 (4) (1999) 448–454.
- [6] M. Sahmaran, G. Yildirim, T.K. Erdem, Self-healing capability of cementitious composites incorporating different supplementary cementitious materials, Cement Concr. Compos. 35 (1) (2013) 89–101.
- [7] A. Alyousif, M. Lachemi, G. Yildirim, M. Şahmaran, Effect of self-healing on the different transport properties of cementitious composites, J. Adv. Concr. Technol. 13 (3) (2015) 112–123.
- [8] M. Şahmaran, S.B. Keskin, G. Ozerkan, I.O. Yaman, Self-healing of mechanically-loaded self-consolidating concretes with high volumes of fly ash, Cement Concr. Compos. 30 (10) (2008) 872–879.
- [9] E. Özbay, M. Šahmaran, M. Lachemi, H.E. Yücel, Self-healing of microcracks in high-volume fly-ash-incorporated engineered cementitious composites, ACI Mater. J. 110 (1) (2013) 33–43.
- [10] Z.G. Zhang, S.Z. Qian, H. Ma, Investigating mechanical properties and self-healing behavior of micro-cracked ECC with different volume of fly ash, Constr. Build. Mater. 52 (2) (2014) 17–23.
- [11] L.L. Kan, H.S. Shi, A.R. Sakulich, V.C. Li, Self-healing characterization of engineered

- cementitious composite materials, ACI Mater. J. 107 (6) (2010) 617-624.
- [12] Y. Yang, M.D. Lepech, E.H. Yang, V.C. Li, Autogenous healing of engineered cementitious composites under wet–dry cycles, Cement Concr. Res. 39 (5) (2009) 382–390.
- [13] Y. Yang, E.H. Yang, V.C. Li, Autogenous healing of engineered cementitious composites at early age, Cement Concr. Res. 41 (2) (2011) 176–183.
- [14] V.C. Li, C.K. Leung, Steady-state and multiple cracking of short random fiber composites, J. Eng. Mech. 118 (11) (1992) 2246–2264.
- [15] V.C. Li, D.K. Mishra, H.C. Wu, Matrix design for pseudo-strain-hardening fibre reinforced cementitious composites, Mater. Struct. 28 (10) (1995) 586–595.
- [16] V.C. Li, S. Wang, C. Wu, Tensile strain-hardening behavior of PVA-ECC, ACI Mater. J. 98 (6) (2001) 483-492
- [17] Z. Zhang, Q. Zhang, Matrix tailoring of Engineered Cementitious Composites (ECC) with non-oil-coated, low tensile strength PVA fiber, Constr. Build. Mater. 161 (2018) 420–431.
- [18] M. Li, V.C. Li, High-early-strength engineered cementitious composites for fast, durable concrete repair-material properties, ACI Mater. J. 108 (1) (2011) 3–12.
- [19] Z.G. Zhang, A. Yuvaraj, J. Di, S.Z. Qian, Matrix design of light weight, high strength, high ductility ECC, Constr. Build. Mater. 210 (2019) 188–197.
- [20] E.H. Yang, Y.Z. Yang, V.C. Li, Use of high volumes of fly ash to improve ECC mechanical properties and material greenness, ACI Mater. J. 104 (6) (2007) 620–628.
- [21] M.D. Lepech, V.C. Li, Water permeability of engineered cementitious composites, Cement Concr. Compos. 31 (10) (2009) 744–753.
- [22] Z. Zhang, S. Qian, H. Liu, V.C. Li, Ductile concrete material with self-healing capacity for jointless concrete pavement use, Transport. Res. Rec.: J. Transport. Res. Board (2640) (2017) 78–83.
- [23] M. Sahmaran, M. Li, V.C. Li, Transport properties of engineered cementitious composites under chloride exposure, ACI Mater. J. 104 (6) (2007) 303–310.
- [24] M. Li, V.C. Li, Cracking and healing of engineered cementitious composites under chloride environment, ACI Mater. J. 108 (3) (2011 May 1) 333–340.
- [25] H. Ma, S. Qian, Z. Zhang, Effect of self-healing on water permeability and mechanical property of medium-early-strength engineered cementitious composites, Constr. Build. Mater. 68 (2014) 92–101.
- [26] S.Z. Qian, J. Zhou, E. Schlangen, Influence of curing condition and precracking time on the self-healing behavior of engineered cementitious composites, Cement Concr. Compos. 32 (9) (2010) 686–693.
- [27] E.N. Herbert, V.C. Li, Self-healing of microcracks in engineered cementitious composites (ECC) under a natural environment, Materials 6 (7) (2013) 2831–2845.
- [28] G. Yildirim, M. Sahmaran, H.U. Ahmed, Influence of hydrated lime addition on self-healing capability of high volume fly ash incorporated cementitious composites, ASCE J. Mater. Civil Eng. 27 (6) (2015) 1–11.
- [29] Z.G. Zhang, Q. Zhang, Self-healing ability of Engineered Cementitious Composites (ECC) under different exposure environments, Constr. Build. Mater. 156 (2017) 142–151.
- [30] H. Ma, E. Herbert, M. Ohno, V.C. Li, Scale-linking model of self-healing and stiffness recovery in Engineered Cementitious Composites (ECC), Cement Concr. Compos. 95 (2019) 1–9.
- [31] J. Qiu, W.L. Aw-Yong, E.H. Yang, Effect of self-healing on fatigue of engineered cementitious composites (ECCs), Cement Concr. Compos. 94 (2018) 145–152.
- [32] D.B. Marshall, B.N. Cox, A J-integral method for calculating steady-state matrix cracking stresses in composites, Mech. Mater. 7 (2) (1988) 127–133.
- [33] E.H. Yang, S.X. Wang, Y.Z. Yang, V.C. Li, Fiber-bridging constitutive law of engineered cementitious composites, J. Adv. Concr. Technol. 6 (1) (2008) 181–193.
- [34] T. Kanda, V.C. Li, A new micromechanics design theory for pseudo strain hardening cementitious composite, J. Eng. Mech. ASCE 125 (4) (1999) 373–381.
- [35] Z. Lin, T. Kanda, V.C. Li, On interface property characterization and performance of fiber reinforced cementitious composites, Concr. Sci. Eng. RILEM (1) (1999) 173–184.
   [36] C. Redon, V.C. Li, C. Wu, H. Hoshiro, T. Saito, A. Ogawa, Measuring and modifying in-
- [36] C. Redon, V.C. Li, C. Wu, H. Hoshiro, T. Saito, A. Ogawa, Measuring and modifying interface properties of PVA fibers in ECC matrix, ASCE J. Mater. Civil Eng. 13 (6) (2001) 399–406.
- [37] Z. Zhang, J. Hu, H. Ma, Feasibility study of ECC with self-healing capacity applied on the long-span steel bridge deck overlay, Int. J. Pavement Eng. (2017) 1–10, https://doi.org/ 10.1080/10298436.2017.1356173.
- [38] H. Ma, Z. Zhang, B. Ding, X. Tu, Investigation on the adhesive characteristics of Engineered Cementitious Composites (ECC) to steel bridge deck, Constr. Build. Mater. 191 (2018) 679–691.
- [39] Z. Zhang, Q. Zhang, S. Qian, V.C. Li, Low E modulus early strength engineered cementitious composites material: development for ultrathin whitetopping overlay. Transport. Res. Rec.: J. Transport. Res. Board (2481) (2015) 41–47.
- [40] E.B. Pereira, G. Fischer, J.A. Barros, Hybrid fiber reinforcement and crack formation in Cementitious Composite Materials, Proceedings of High Performance Fiber Reinforced Cement Composites, vol 6, Springer, 2012, pp. 535–542.
   [41] V.C. Li, C. Wu, S.X. Wang, A. Ogawa, T. Saito, Interface tailoring for strain-hardening
- [41] V.C. Li, C. Wu, S.X. Wang, A. Ogawa, T. Saito, Interface tailoring for strain-hardening polyvinyl alcohol-engineered cementitious composite (PVA-ECC), ACI Mater. J. 99 (5) (2002) 463–472.
- [42] Z. Zhang, Y. Ding, S. Qian, Influence of bacterial incorporation on mechanical properties
- of engineered cementitious composites (ECC), Constr. Build. Mater. 196 (2019) 195–203.
  [43] ASTM C109, Standard Test Method for Compressive Strength of Hydraulic Cement Mortars, (2014).
- [44] S. Fan, M. Li, X-ray computed microtomography of three-dimensional microcracks and self-healing in engineered cementitious composites, Smart Mater. Struct. 24 (1) (2014) 015021
- [45] T. Horikoshi, A. Ogawa, T. Saito, H. Hoshiro, G. Fischer, V. Li, Properties of Polyvinylalcohol fiber as reinforcing materials for cementitious composites, Proceedings of International RILEM Workshop on HPFRCC in Structural Applications, 2006 Honolulu, HI.
- [46] Y.W. Chan, Fiber/Cement Bond Property Modification in Relation to Interfacial Microstructure, Department of Civil and Environmental Engineering, University of Michigan, Ann Arbor, MI, 1994.
- [47] S.X. Wang, V.C. Li, Engineered cementitious composites with high-volume fly ash, ACI Mater. J. 104 (3) (2007) 233–241.